

## Lattice transformations in the approximant and decagonal phases

This article has been downloaded from IOPscience. Please scroll down to see the full text article.

1992 J. Phys.: Condens. Matter 4 7025

(<http://iopscience.iop.org/0953-8984/4/34/003>)

View [the table of contents for this issue](#), or go to the [journal homepage](#) for more

Download details:

IP Address: 171.66.16.96

The article was downloaded on 11/05/2010 at 00:26

Please note that [terms and conditions apply](#).

## Lattice transformations in the approximant and decagonal phases

Song Seng Kang and Jean Marie Dubois

Laboratoire de Science et Génie des Matériaux Métalliques (CNRS URA 159), Ecole des Mines, Parc de Saurupt, F-54042 Nancy Cédex, France

Received 16 March 1992, in final form 8 May 1992

**Abstract.** A few two-dimensional approximant–approximant and approximant–quasicrystal lattice transformations are studied. These lattice transformations are governed by three mechanisms: translational slip, rotational slip and irrational twinning. These operations can generate an infinite number of approximants, most of them having commensurate structure. The irrational twinning generates either the one-dimensional or two-dimensional aperiodic lattices depending on the orientation of the irrational twin plane with respect to the periodic lattice. Experimental evidence in favour of such lattice transformations is supplied by high-resolution electron microscopy imaging in two approximant structures.

### 1. Introduction

The decagonal phase is a quasicrystal built by periodic stacking of two-dimensional (2D) aperiodic atomic layers [1]; it is often described by the Penrose tiling (PT) pattern [2], an array displayed by three (prolate rhombus, convex and concave pentagons) tiling units. Most of the decagonal quasicrystals are metastable at room temperature, e.g. in the Al–Mn [1], Al–Mn–Ni [3] and Al–Cu–Fe–Cr [4] alloy systems. Only a few exceptions are stable either at high temperature, for example in the Al–Cu–Co case [5–7], or at room temperature in the Al–Pd–Mn alloys [8]. The metastable and high-temperature stable quasicrystals transform to their approximant phases after slow cooling or certain heat treatment. Their relationship with the approximant phases have been studied by many authors. Most often, this relationship is discussed within the cut and projection scheme [9], starting from a 5D hyperspace adapted to the decagonal and related approximant phases [10]. The main feature that was pointed out is that both structure types, approximant or quasicrystal, are constructed by the same types of 2D tiling units when viewed along the tenfold or pseudo tenfold directions [6, 7, 11]. The case of icosahedral phase approximants is dealt with in papers quoted in [10]. These phases, which are 3D aperiodic compounds, are beyond the scope of the present paper.

A single-crystal x-ray structure analysis of decagonal  $d\text{-Al}_{65}\text{Cu}_{20}\text{Co}_{15}$  [5] was performed recently using the 5D approach by Steurer and Kuo [12]. The 3D decagonal structure consists of two distinct quasiperiodic layers but related by a tenfold screw axis. They are stacked periodically one upon the other. A pentagonal network linking the atoms in these layers can be drawn. It has an edge length of 2.9 Å. We shall refer

to it as a B-type layer, as in another paper [13] specifically devoted to this subject. A very similar B-type layer is found at height  $y = 1/4$  in the  $\text{Al}_{13}\text{Fe}_4$  [14] lattice, although the perfect tenfold rotational symmetry is broken. Another type of layer, hereafter called A-type as in [13], is observed in  $\text{Al}_{60}\text{Mn}_{11}\text{Ni}_4$  [15]: it is characterized by a pentagonal network with edge length  $\tau \times 2.9 \text{ \AA}$  where  $\tau$  is the golden mean.

We have shown in [13] that these two types of layers, as well as the layers related to each of them by a screw axis obeying the tenfold symmetry, may be used to construct all quasicrystalline structures as well as the approximant ones. The principle consists of recovering the 3D space dimensionality by stacking along the tenfold axis (or pseudo tenfold axis) the 2D A and B types of layers according to selection rules defined by stereo-topological constraints. This principle is not different from the one which rules polytypes, e.g. FCC versus HCP lattices.

In this paper we consider only the transformations that may occur within one given structure, either quasicrystalline or approximant. The stacking sequence is therefore defined and is not supposed to change during transformation. Thus we may restrict ourselves to the crystallographic transformations that occur inside a given layer, e.g. the A-type network.

For the sake of simplicity of the drawings, we shall focus attention on one single layer, assuming that the layers above and below it undergo the same crystallographic transformation.

The structure transformation may involve shear, slip or twinning mechanisms which are often assigned to the incorporation of point defects such as vacancies and interstitials in connected coordination polyhedra. In the case of crystals, many 2D lattice transformations related to these defects have been discovered by Hyde *et al* [16]. A pictorial model for solid-state amorphization based on a disordered partition of interstitial atoms in octahedral sites of the HCP lattice (the so-called chemical twinning introduced by Andersson and Hyde in 1974 [17]) has been demonstrated by Dubois [18].

The formation of approximant crystalline structure from quasicrystalline phase is always related to the action of phason strains. It has been shown by Zhang and Kuo [19] that, introducing phasons in two orthogonal directions in the quasiperiodic plane perpendicular to the periodic tenfold axis, the Penrose pattern progressively becomes a large periodic lattice. The corresponding simulated electron diffraction patterns agree fairly well with experiments. In another approach, Dong and Dubois [20] have tackled the transformations by twinning operations and proposed a 2D geometrical model for the decagonal phase. This model uses the tenfold twinning operation to multiply the atomic clusters with tenfold symmetry. The basic structure units, from which the observed units can be constructed, have been found to be the Robinson triangles. An alternative approach to the approximant and quasicrystalline structures was introduced in a previous paper [13] where the structure description has been lifted to atomic scale by identifying the cluster units decoration with the help of a known crystalline structure. In this paper, attention will be focused on the mechanism which causes the formation of either periodic or aperiodic arrays. After explanations of several approximant structures in section 3, three examples of the lattice transformations will be given in section 4. The first one concerns the linear slip operation between two periodic lattices without change in unit cell area during transformation. The second example reveals a new rotational slip (rotated around an axis of pseudo tenfold symmetry or tenfold symmetry). Irrational twinning (the twin plane is characterized by an irrational cut of the 2D periodic lattice) involved in

the lattice transformation between periodic and 1D-aperiodic or 2D-aperiodic lattices will be introduced in the last case.

All phases on which we report below are looked at in relation only to the lattice perpendicular to the tenfold or pseudo tenfold directions tiled with units having edge length  $d \approx 4.6 \text{ \AA}$ . Our discussion will deal with crystallographic transformations relating the tilings to each other. At present, computer simulation work is in progress to understand such transformations in terms of phase transitions, using effective pair potential data.

## 2. Experimental details

In order to substantiate the lattice transformations proposed in the following, a high-resolution electron microscopy study was performed on real approximant crystals.

Three alloys of nominal compositions as indicated below were prepared by induction melting of pure elements under helium atmosphere. They were drawn in the liquid state into cylindrical moulds and cooled to room temperature at a rate of about  $5 \times 10^2 \text{ K s}^{-1}$ .

alloy A— $\text{Al}_{80.75}\text{Mn}_{13.75}\text{Ni}_{5.5}$  (at.%)

alloy B— $\text{Al}_{67}\text{Cu}_9\text{Fe}_{10.5}\text{Cr}_{10.5}\text{Si}_3$  (at.%)

alloy C— $\text{Al}_{62.5}\text{Cu}_{18.5}\text{Fe}_8\text{Cr}_8\text{Si}_3$  (at.%)

The alloy A was rapidly cooled by the melt spinning method on a copper wheel rotating at a tangential speed of the cooling surface of  $V = 12 \text{ m s}^{-1}$ . The as-cast cylindrical samples of the alloys B and C were compressed at room temperature up to fracture stress  $\sigma = 555 \text{ MPa}$  and at  $800 \text{ }^\circ\text{C}$  under argon atmosphere till the strain reached  $\epsilon = 0.2$ . These samples will be called samples A, B and C respectively. The structure analysis was realized by using the transmission electron microscope (TEM) JEOL-200CX on powder samples prepared by crushing bits of the alloys.

## 3. Structure of several important orthorhombic approximants

The structure details of the approximant phases reported so far are insufficiently specified, especially for those with large unit cells. Thus, in the following subsections, we will present three types of large approximant structure which are closely related with the decagonal phase.

### 3.1. $(4_v2_p)$ -type approximant ( $\Sigma$ phase and $\varphi$ phase)

Two simple patterns that can be displayed by the convex pentagon and prolate rhombus tiling units are schematized in figure 1. These patterns reproduce the atomic decoration of the layers lying on the mirror plane ( $y = 1/4$  or  $3/4$ ) of known crystal structures, namely the  $\Sigma$  phase [21] of composition  $\text{Al}_{61.5}\text{Cu}_{7.5}\text{Fe}_{11}\text{Cr}_{17}\text{Si}_3$  (figure 1(a)) and the  $\varphi$  phase [15] of composition  $\text{Al}_{60}\text{Mn}_{11}\text{Ni}_4$  (figure 1(b)). They are both orthorhombic structures each with unit cell packed by four convex (v) pentagons and two prolate (p) rhombuses. According to the 2D classification scheme proposed previously [13], they belong to  $(4_v2_p)$ -type approximants. The aluminium atoms at pentagon vertices form a sublattice with edge length  $d_A \approx 4.6 \text{ \AA}$  inside the orthorhombic unit cells. This is the essential reason why our attention is only on the sublattice scale for the lattice transformation in section 4. We will come back to these simple lattices when discussing the lattice transformation.

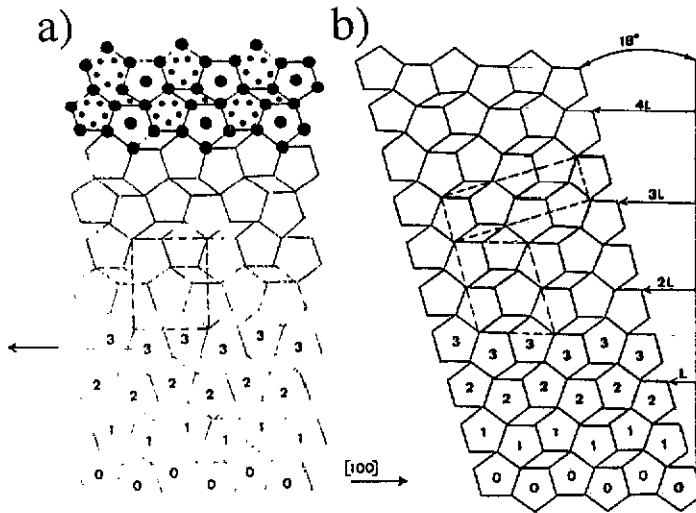


**Figure 1.** Two simple arrays packed by the convex pentagon and prolate rhombus tiling units. (a) The orthorhombic  $\Sigma$  phase ( $\bullet$ —Al atom,  $\bullet$ —transition metals) and (b) the orthorhombic  $\varphi$  phase with the  $\text{Al}_{13}\text{Fe}_4$  monoclinic cell laid out in the middle of the  $\varphi$ -phase lattice.

### 3.2. $(16_v4_c6_p)$ -type approximant ( $O_1$ phase)

Recently van Tendeloo *et al* [3] discovered a decagonal phase in a rapidly cooled sample of composition  $\text{Al}_{60}\text{Mn}_{11}\text{Ni}_4$ . In our sample A, the selected area electron diffraction pattern (SAED) taken along the tenfold direction looks very like the one shown by van Tendeloo *et al* [3] (figure 2(a)). However, a careful analysis of the HREM image proves that the structure is microcrystalline rather than quasicrystalline (figure 2(c)). As indicated by arrows on top of the HREM image, some of the rows are periodically arranged. This image is actually a lattice roughly constructed by the  $\tau^3 d_A$ -type rhombus (see pattern schematized in figure 2(c)). In some areas these rhombuses arrange themselves into a B-face centred orthorhombic lattice with cell parameters  $a = 24.0 \text{ \AA}$ ,  $b = 12.4 \text{ \AA}$  and  $c = 32.7 \text{ \AA}$ . This orthorhombic phase (hereafter the  $O_1$  phase) has already been found in Al-Cu-Fe-Cr alloys (after Dong *et al* [7], this phase has an  $mm2$  point group). Referring to another HREM image taken in the same area as figure 2(c) but with different defocused contrast (see enlarged image shown in figure 2(b)), a sublattice with edge length  $d_A = 4.6 \text{ \AA}$  of the oblate rhombus can be proposed. This pattern is drawn according to the fact that the  $(4_v2_p)$ -type approximant (the  $\varphi$  phase) which is found in the same alloy system is packed by the v-type pentagon with edge length  $d_A$ . Thus, if one supposes that each black point of the HREM image corresponds to a v-type pentagon, then the pattern obtained is unique as shown in figure 2(b). This large oblate rhombus is packed by eight convex (v) pentagons, two concave (c) pentagons and two prolate rhombuses (figure 2(b)). Since the orthorhombic unit cell of the  $O_1$  phase consists of two large oblate rhombuses (figure 2(c)), it is noted as the  $(16_v4_c6_p)$ -type approximant.

A sublattice of a distorted prolate rhombus is also schematized in figure 2(b). This distorted prolate rhombus has two different edge lengths. It can be produced by a slip mechanism applied to a lattice built by the oblate rhombuses (see section 4.4).

It is possible to deduce the space group of the  $O_1$  phase by combining the 2D

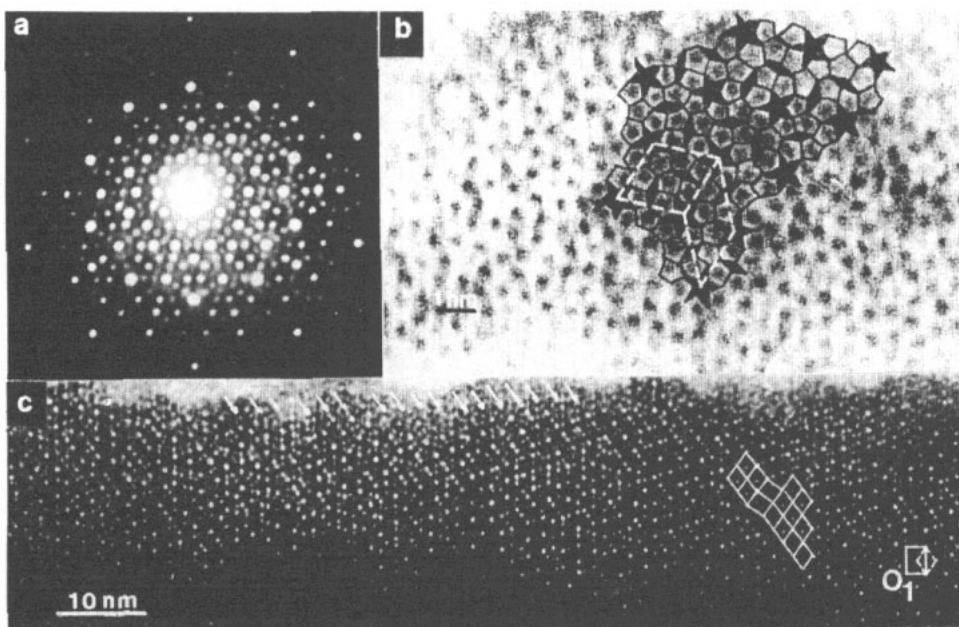


Figure 2. (a) Selected-area electron-diffraction pattern, (b) and (c) HREM images of the  $\text{Al}_{80.75}\text{Ni}_{5.5}\text{Mn}_{13.75}$  alloy. The enlarged HREM image (b) is taken in the same area as (c) with different defocused contrast.

space group deduced from the pattern and the crystallographic symmetry in the third dimension perpendicular to this 2D pattern. We suppose that the mirror plane at  $y = 1/4$  and  $3/4$  of the  $\Sigma$  phase (see figure 1 and [21] for more details on the  $\Sigma$ -phase structure) is the same as in the  $\text{O}_1$ -phase case. Then the space group of the  $\text{O}_1$  phase is obtained as  $Bbm2_1$ . This space group belongs to the point group  $mm2$  reported in [7]. We have applied the same model to decipher the atomic structure of the new Al-Cu-Fe-Cr-Si orthorhombic compound, in agreement with single crystal x-ray diffraction data [21].

### 3.3. $(10_v2_c4_p)$ -type approximant ( $\Omega$ phase)

Several approximant phases have been found in the Al-Cu-Fe-Cr alloys. Most of them have orthorhombic structures, for example the  $\text{O}_1$  phase [4] in alloy  $\text{Al}_{65}\text{Cu}_{20}\text{Fe}_{10}\text{Cr}_5$  (the optimal composition for this  $\text{O}_1$  phase as detected by microprobe electron microscopy is  $\text{Al}_{70}\text{Cu}_9\text{Fe}_{10.5}\text{Cr}_{10.5}$ ) and the  $\Sigma$  phase [21] in alloy  $\text{Al}_{61.5}\text{Cu}_{7.5}\text{Fe}_{11}\text{Cr}_{17}\text{Si}_3$ . In the present investigation, a new orthorhombic phase was discovered in the sample B- $\text{Al}_{67}\text{Cu}_9\text{Fe}_{10.5}\text{Cr}_{10.5}\text{Si}_3$ . This phase (hereafter the  $\Omega$  phase) has a primitive structure with cell parameters  $a = 23.6 \text{ \AA}$ ,  $b = 12.3 \text{ \AA}$  and  $c = 20.0 \text{ \AA}$ . The pseudo tenfold (010) SAED pattern and its corresponding HREM images are given in figure 3. From the high-resolution image (see figure 3(c) and its enlarged image in figure 3(b)), this  $\Omega$  phase is a  $(10_v2_c4_p)$  approximant constructed from ten convex pentagons, two concave pentagons and four prolate rhombuses. By using the same space group determination method as for the  $(16_v4_c6_p)$   $\text{O}_1$  phase (see previous section), the space group can be deduced as  $P2mc$ .

Note that the pseudo tenfold ring observed in the HREM image corresponds to

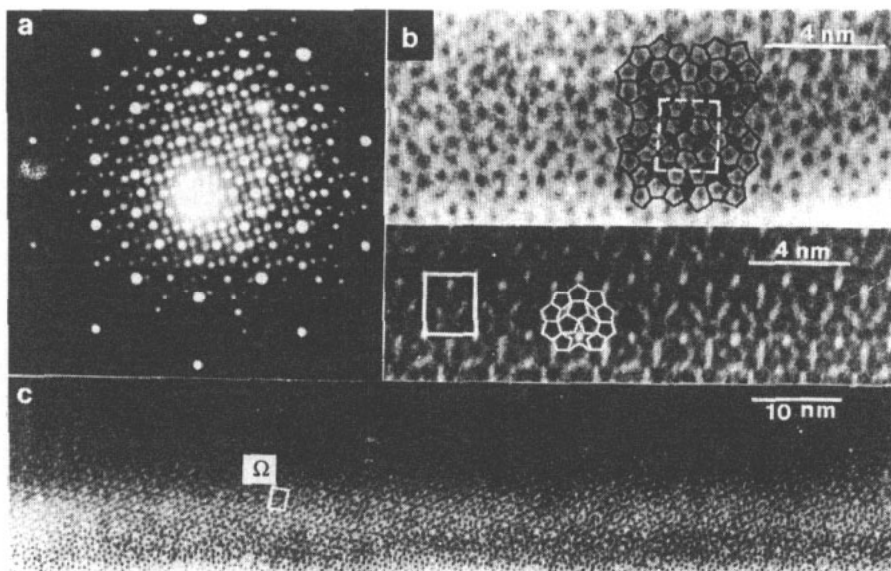


**Figure 3.** (a) Selected-area electron-diffraction pattern, (b) and (c) HREM images taken along the pseudo tenfold direction in the  $\text{Al}_{67}\text{Cu}_9\text{Fe}_{10.5}\text{Cr}_{10.5}\text{Si}_3$  alloy. The top image of (b) is an enlarged image of (c) whereas the bottom image of (b) is taken in the same area as (c) with different defocused contrast.

the pentagon ring laid out in the bottom of figure 3(b). This HREM contrast can be changed to a white-dot-type contrast without the presence of pseudo tenfold rings (see figure 2(c) for example). The centred point of the star-like unit (bottom image of figure 3(b)) corresponds to an intense dot. The pattern laid out by connecting the intense points may then be different from the one obtained by connecting pseudo tenfold rings (this point has been illustrated in [7]).

#### 4. Tilings and lattice transformations

##### 4.1. Tiling condition and notations

The tiling condition that we will introduce here is quite similar to matching rules [22]. However, in our case, the tiling units are not the oblate and prolate rhombuses as usually used in the literature but are convex pentagon, concave pentagon and prolate rhombus labelled as *v* unit, *c* unit and *p* unit, respectively.

From the lattices schematized in figures 1, 2 and 3, we can see that the *v* unit is the principal tiling unit. It is always present in first-neighbour positions of the other tiling units i.e. the *c* unit and *p* unit. This means that the first-neighbour tiling configuration for each unit can then be characterized by the number of *v*-type pentagons located in its first-neighbour shell. We summarize the possible tiling configurations for each basic tiling element (i.e. *v*, *c* and *p* units) in table 1. The notation given in the central column of table 1, for example  $4p_1$  denotes the number of *v*-type units (here four) placed in the first neighbour position of the *p* unit which has one atom inside.

As can be seen in figure 1, convex pentagons have two different atomic configurations. One has only one atom lying at the centre of the pentagon and the other has

five atoms near the edges of the pentagon. These will be denoted  $v_1$  and  $v_5$  respectively (table 1). In fact, the  $c$  unit and  $p$  unit also have different atomic configurations. Depending on the type of  $v$  unit i.e.  $v_1$  or  $v_5$ , placed in the first-neighbour position, the  $c$  unit can be distinguished as  $c_0$  (no atom inside the unit) or  $c_2$  (two atoms inside the unit). The  $p$  unit yields only a change in atomic position, with one atom being on the top and another on the bottom of the unit (table 1, see two  $2p_1$  configurations for example). Thus, each independent pattern has a dual packing (e.g.  $3c_0$  and  $3c_2$ ). The same kind of tiling units, for example  $v$  units, cannot be connected to each other without using an intermediate tiling unit such as a  $p$  unit or a  $c$  unit, due to the existence of stereological constraints [13]: two  $v_1$  pentagons together would produce a too-loosely-packed array whereas two-edge connected  $v_5$  units involve unphysically short pair distances. This tiling condition will be used to determine which lattice transformation avoids the existence of stereological constraints.

**Table 1.** Basic tiling elements and first-neighbour tiling condition. All first-neighbour tiling patterns have a dual packing. Two examples are given in the table,  $2p_1$  and  $3c-3c_2$ . The notation denotes the number of atoms in a tiling unit and the number of  $v$ -type pentagons in the first-neighbour position (e.g.  $3v_5$  has three  $v$ -type pentagons surrounding a  $v$ -type pentagon which has five atoms).

Tiling element	First neighbour tiling conditions	Three dimensional tiling unit
Prolate rhombus  $p$		
Concave pentagon  $c$		
Convex pentagon  $v$		



#### 4.2. Translational slip as a lattice transformation operation in a $(4_v 2_p)$ -type approximant

To illustrate how the linear slip operation intervenes as a mechanism of structure transformation, we select here as an example a simple transformation between two close approximant arrays: the  $\Sigma$  and  $\varphi$  phases. The coexistence of these two structures has been observed by Daulton *et al* [23] in Al-Mn alloys. However, the atomic decorations of the isostructural phases  $\Sigma$  and  $\varphi$  in the  $\text{Al}_{74}\text{Mn}_{26}$  alloys may be different from the ones observed in the  $\text{Al}_{61.5}(\text{Cu-Fe-Cr-Si})_{38.5}$  and  $\text{Al}_{80}(\text{Ni-Mn})_{20}$  alloys respectively, due to the difference in compositions. As a matter of fact, these two lattices are not transformed from each other by the twinning operation as described by Daulton *et al* [23] but rather by the slip operation.

The slip operation can be illustrated in the sublattice scale with edge length  $d \approx 4.6 \text{ \AA}$  (figure 1). The approximant structures show a gliding of every two pentagon chains (denoted 1 and 2 in figure 1) along the direction [100] for a distance  $d_A = L = a/\tau^2$  and an angle  $18^\circ$ , where  $a$  is the cell parameter of the  $\Sigma$  phase and  $\tau = (\sqrt{5} + 1)/2$ . The orthorhombic  $\Sigma$  unit cell (figure 1(a)) is distorted to a monoclinic unit cell (figure 1(b)) and vice versa.

#### 4.3. Rotational and screw rotational slips

In the previous example we pointed out how translational slip may rearrange pentagonal tilings. The present section is devoted to another type of rearrangement. Instead of gliding between two pentagon chains, the gliding is now governed by the rotation of three pentagons located inside a ring of nine pentagons and is restricted around a local rotational axis defined by the pseudo tenfold axis. The angular increment is taken as  $n\pi/5$  to satisfy the tiling condition given in table 1, where  $n$  is integer. This kind of gliding is called rotational slip (for more details on this operation see Hyde *et al* [24]).

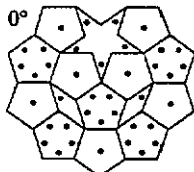
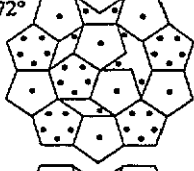
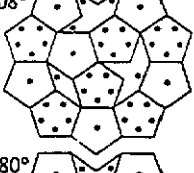
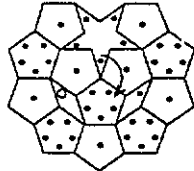
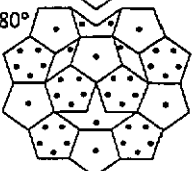
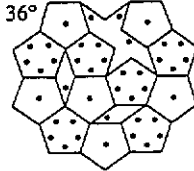
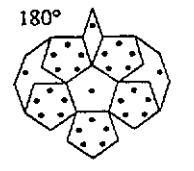
Table 2 gives all the possible configurations for clockwise rotational mode from angle  $0^\circ$  to  $180^\circ$ . This configuration of  $0^\circ$  is considered as the initial ring configuration. For  $n = \text{odd integer}$ , the configurations (e.g.  $36^\circ$  mode) have two more atoms than the initial ring configuration. In the contrary cases ( $n = \text{even integer}$ ), the atomic density of the configurations is the same as the initial one. This means that both rotational modes ( $n = \text{odd or even}$ ) result from the different nature of the rotational slip. However, for the sequential transformation from one lattice to another to be possible, the rotation operation must permit generation of new sets of pentagon rings. Only  $4\pi/5 = 144^\circ$  ( $n = 4$ ) and  $\pi/5 = 36^\circ$  ( $n = 1$ ) satisfy this criteria and they will be used in the following to realize the lattice transformations.

The  $4\pi/5$  rotations (clockwise and anticlockwise) are considered as planar rotations because there is no change of atomic density in the pentagon ring configuration. Since metallic materials pretend to close packing, this rotational slip may result from the incorporation of substitutional atoms between small atoms and large atoms inside the tiling units. If this is true then the generated approximant phases may have different compositions. This assumption is based on the fact that most of the approximant phases existing in an alloy system have different compositions (for example, as quoted in section 3.3, the  $O_1$  phase was found in alloy  $\text{Al}_{70}\text{Cu}_9\text{Fe}_{10.5}\text{Cr}_{10.5}$  whereas the  $\Omega$  phase and  $\Sigma$  phase were discovered in  $\text{Al}_{67}\text{Cu}_9\text{Fe}_{10.5}\text{Cr}_{10.5}\text{Si}_3$  and  $\text{Al}_{61.5}\text{Cu}_{7.5}\text{Fe}_{11}\text{Cr}_{17}\text{Si}_3$  respectively).

To illustrate how the atom shifts from one configuration to another, we suppose that the substitutional atom is located inside the prolate rhombus (see centre-left

column of table 2). During rotation, this misplaced substitutional atom moves to the star-like unit for a new configuration. The whole operation is schematized in the centre-left column of table 2.

Table 2. Rotation conditions and rotational slips in the pentagon ring.

Possible rotation patterns	Rotational slip	Screw rotational slip	Reflected screw rotational slip
<p>0°</p> 			
<p>72°</p> 			
<p>108°</p> 	<p>144°</p> 		
<p>180°</p> 		<p>36°</p> 	
			<p>180°</p> 

In the  $\pi/5$  case, the rotation may involve local stacking faults in the third dimension of the lattice (table 2, centre-right column). The term 'local stacking fault' is introduced here because the defect is only present inside the pentagon ring. This may be due to the absence of two atoms lying in the star-like tiling unit (see marks '+'). The atoms occupying sites in the layer just above or below (see marks ' $\Delta$ ') will then be able to displace themselves to fill these vacancies. The atomic configuration above or below the 2D layer is different. For instance, if one considers the configurations of the 3D units as being the cluster units packing the  $\Sigma$ -phase lattice, then five atoms or one atom respectively are located above or below the  $v_1$  or  $v_5$  units (see table 1). After replacement, the  $v_5$  pentagon transforms to  $v_1$  and vice versa (table 2). This leads to the three pentagons placed at the centre of the pentagon ring being rotated by  $\pi/5$  to accommodate the allowed configuration given in table 1. The whole process is then call 'screw rotational slip'.

The screw rotational slip operation is not necessarily limited to the inside of the pentagon ring. After rotation by 180°, it can be operated in a tiling fragment in which a convex pentagon is placed between a concave pentagon and a prolate rhombus as schematized in the right-hand column of table 2. This operation may happen when four atoms are simultaneously missing from the star-like unit. Thus there are two

symmetrical slips operating over two sides of the star-like unit. This operation is called 'reflected screw rotational slip'.

#### 4.4. Lattice transformations

As displayed by the HREM image in figure 4, the  $(16_v4_c6_p)$ - $O_1$  and  $(10_v2_c5_p)$ - $\Omega$  approximant lattices share common crystallographic directions (e.g.  $[100]_{O_1} \parallel [100]_{\Omega}$ ). These lattices can be transformed into each other by rotational slip in a clockwise direction around the  $b$ -axis inside the pentagon rings of the  $O_1$  pattern (figure 5(a-d)). For the sake of illustration, and to keep close to the HREM image (figure 4), the initial lattice of the  $O_1$  phase is separated into two parts (see broken line) in figure 5(a). The left-hand area remains unchanged whereas all the rings situated in the right-hand area undergo the rotational slip operation. This operation generates another set of pentagon rings between the former positions of the pentagon rings. A substructure of the  $O_1$  phase is obtained after the first application of the rotational slip operation (broken lined cell on the right-hand side of figure 5(b)). Then the rotational slip may take place again in this second set of rings (figure 5(b)). Note that other rotational modes, e.g.  $72^\circ$  as given in table 1, cannot form a new set of pentagon rings after the first operation. This second step forms a column of  $\Omega$ -cells in the area neighbouring the  $O_1$  lattice at the left-hand side (figure 5(c): the present configuration is identical to the lattice pattern marked with A in the HREM image of figure 4 if one considers that each intense dot in the HREM image corresponds to the star-like unit). If these operations are repeated, then a large area of the  $\Omega$  phase (as e.g. the area marked B in figure 4) is obtained (figure 5(d)). The growth of the  $\Omega$  phase is governed by the subsequent rotational slip process in the  $O_1$  lattice. In contrast to the lattice transformation governed by the translational slip operation (section 4.2), the lattice transformation proceeding by the planar rotational slip is a slow process since it needs two steps to form a column of  $\Omega$  cells.

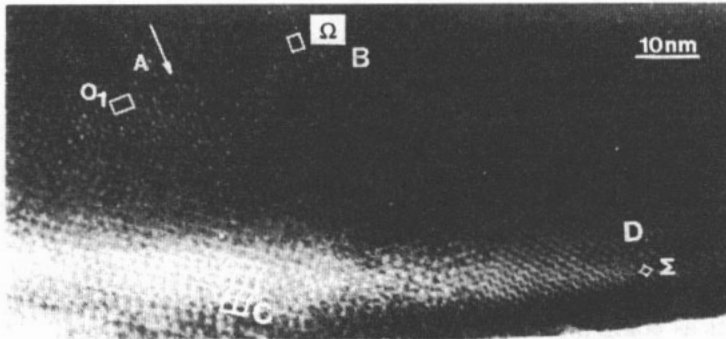


**Figure 4.** HREM image showing the coexistence of three orthorhombic phases:  $O_1$ ,  $\Omega$  and  $\Sigma$ .

The formation of the  $\Omega$  phase is, however, not the last state of transformation achieved by rotational slip. For instance, this may be due to the ordering system of the substitutional atoms which repeat every five different positions in the star-like unit (see figure 5(d)). If one continues the same slip operation in this  $\Omega$ -phase lattice, an infinite series of orthorhombic approximant phases, for example the B-face centred orthorhombic phase schematized in figure 5(e), will be generated. These approximant phases are commensurate structures. A simple sublattice (without a pentagon ring,

here the  $\varphi$  phase,  $(4_v 2_p)$ -type approximant) is formed with an orthorhombic unit cell as shown in figure 5(f). This simple approximant phase is stable with respect to rotational slip that can only be operated when the pentagonal rings are present. Nevertheless, the  $\varphi$ -phase lattice can be transformed back to the  $\Sigma$ -phase lattice if the translational slip operation mentioned in the first example (figure 1) is applied. The area D in figure 4 shows the occurrence of such a case.

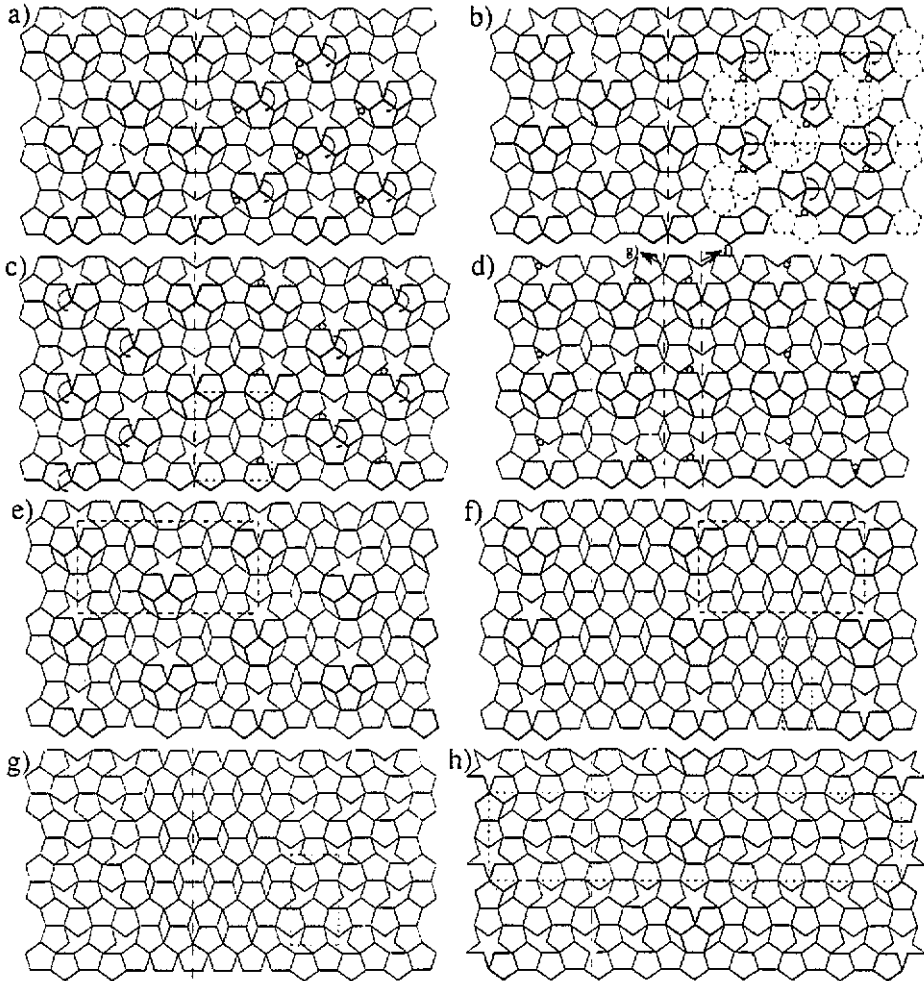


**Figure 5.** (a)–(d) The lattice transformation process operated by the clockwise rotational slip from the  $O_1$  lattice to the  $\Omega$  lattice. (e), (f) Two commensurate structures with  $\varphi$ -phase sublattices. (g) Coexistence of the  $\varphi$ -phase lattice and the  $(6_v 2_c 2_p)$ -approximant lattice obtained from the symmetrical rotational slip operated at the centre of the  $\Omega$  cells (see (d)). (h) A large face-centred orthorhombic commensurate structure obtained from the anticlockwise rotational slip with the  $(6_v 2_c 2_p)$  sublattice. The basal axis (broken lines) is  $[001]-O_1$ .

Each approximant phase has a substructure as shown in figures 5(a) and (b) except the simple-type approximant structures which have no pentagon rings, e.g. the  $(4_v 2_p)$ -type structures (figure 5(f)).

The commensurate structure is not necessarily formed if the rotational slip operation is operating symmetrically in the  $\Omega$  lattice with basal axis marked  $g$ ) in figure 5(d) placed at position  $c/2$  where  $c$  is the cell parameter of the  $\Omega$  phase. The formation of both  $\varphi$  or  $\Sigma$  phases rejects the foreign atoms (figure 5(g)) causing a change in stoichiometry and forming another orthorhombic ( $6_v2_c2_p$ )-type approximant in the same sample.

Through anticlockwise rotation, another infinite series of approximant phases is also formed. However, this time the sublattice of the commensurate structure is the ( $6_v2_c2_p$ )-type approximant (figure 5(h)).

For each independent axis chosen for each large approximant phase, the rotational slip process always gives an infinite number of different approximant phases with a more simple lattice produced inside the large approximant arrays. The generated lattices are not limited to only the orthorhombic structures. A series of monoclinic lattices can also be obtained if the basal axis is  $[101]-O_1$ .

Each lattice formation has its own growth rate because of the variation of unit-cell surface. For example, the  $O_1-\Omega$  transformation is faster than the  $\Omega-\varphi$  transformation.

The presence of area C in the HREM image shown in figure 4 demonstrates that the  $O_1-\Omega$  lattice transformation can also proceed along the  $[101]-O_1$  direction. We have mentioned before that in this direction a series of monoclinic cells will be obtained if the planar slip operation is applied. Indeed, the  $O_1-\Omega$  transformation along this direction can involve another mode of mechanism: the screw rotational slip.

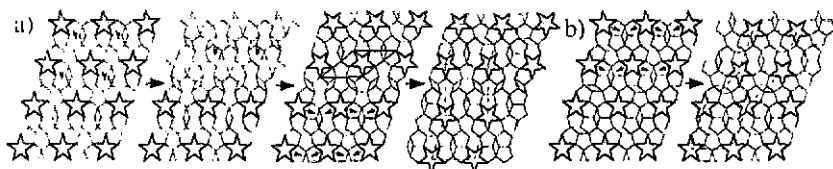


**Figure 6.** (a) Formation of  $\Omega$  cells (right-hand side) by a  $36^\circ$  screw rotational slip (left and centre-left) followed by reflected screw rotational slip (centre-right) in the  $O_1$  lattice along the  $[101]-O_1$  direction. (b) Formation of distorted large prolate rhombuses by reflected screw rotational slip.

Figure 6(a) shows the corresponding  $O_1-\Omega$  transformation process. The lattice transformation is generated by screw rotation by an angle of  $36^\circ$  in the upper part of figure 6(a) (left-hand side). Meanwhile the bottom part of the figure is provisionally kept unchanged for clarity. After two steps, the reflected screw rotation is applied to the bottom part of the same figure (middle-right side of figure 6(a)). During this lattice transformation, a column of perfect prolate rhombuses (obtained from the connection of pentagon rings) which can usually be drawn out in the HREM image is obtained (figure 6(a) middle-right lattice).

Another example concerning only the reflected screw slip is presented in figure 6(b). The lattice transformation is generated by the slip in the upper part of figure 6(b) (left-hand side). The generated part of the large distorted prolate rhombus (right-hand side of figure 6(b)) coincides with the pattern schematized on the HREM image of figure 3(b). This distorted prolate rhombus has two different edge lengths.

#### 4.5. Lattice transformation between approximant and quasicrystals

**4.5.1. Irrational twinning.** The large pentagon with edge length  $\tau^3 d_A$  which is usually observed in the HREM image cannot be generated by the rotational slip operated in the usual way as illustrated in the above examples. It is also unrealizable by the classical lattice twinning reported so far and concerning only the rational plane of the periodic lattice [19]. However, we show in this section that a large pentagon can be obtained by a simple 'irrational twinning operation'.

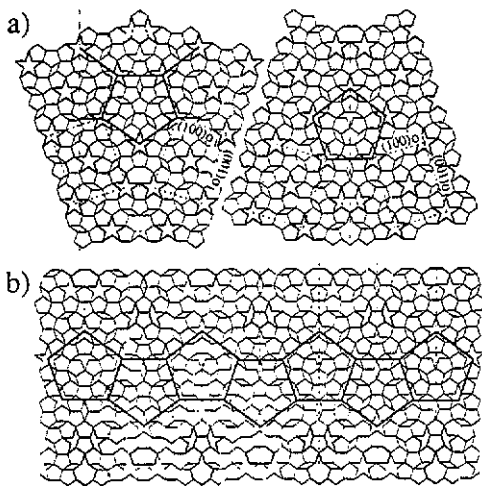
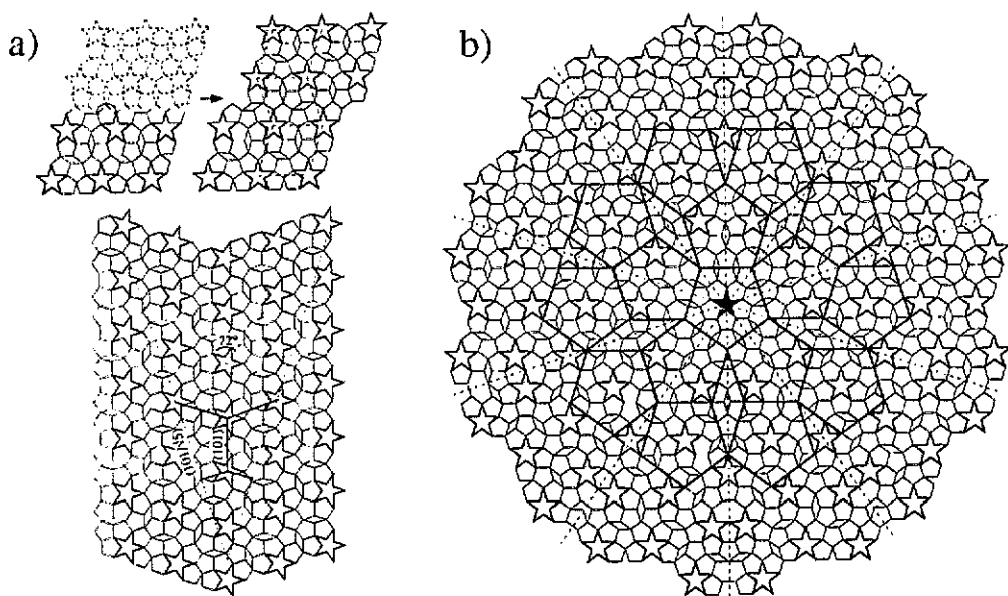


Figure 7. (a) Irrational twinning performed in the  $O_1$  lattice with the twin plane  $(101/\sqrt{5})$  being  $-18^\circ$  and  $+18^\circ$  off the  $(001)-O_1$  direction at the left- and right-hand sides respectively. (b) One dimensional lattice as generated from a periodic sequence of irrational twinnings applied in the  $O_1$  lattice.

The concept of irrational twinning is the same as classical lattice twinning except that now the lattice twinning has an irrational twin plane cut through the periodic lattice. Since the sublattice of the approximant phase has a pentagonal decoration, some of the planes thus generated, called the irrational atomic planes, are positioned in irrational directions. This makes the twinning realizable in these irrational atomic planes. Figure 7(a) shows two examples of irrational lattice twinning operations applied to the  $(16_v 4_c 6_p)$  lattice. One has an angle of  $-18^\circ$  (figure 7(a) left-hand side) and another  $+18^\circ$  (figure 7(a) right-hand side) apart from the  $[100]-O_1$  axis. The twin plane is  $(10L)_{O_1}$ , with  $L = a \tan 18^\circ = c \tan 18^\circ / \tan 36^\circ = 1/\sqrt{5}$  where  $a$  and  $c$  are unit cell parameters of the  $O_1$  phase. Note that there is only one unit-cell vertex placed on this twin plane.

**4.5.2. Formation of one-dimensional and decagonal quasicrystals.** The description for the formation of 1D or 2D quasicrystals begins with the  $(16_v 4_c 6_p)$  lattice. We select this lattice as the starting field because it is a close approximant of the decagonal quasicrystal [15]. However, the present concept can be applied in any approximant lattice, except that the tiling pattern will be different. The decagonal pattern obtained by irrational twinning is not universal since there are different starting lattices that may be considered although all of them yield tenfold symmetry.

When the periodic sequence of irrational twinning occurs in this lattice, the lattice so obtained is 1D quasiperiodic lattice. It forms an aperiodic packing parallel to the



**Figure 8.** (a) Translational slip applied in the  $O_1$  lattice along the  $[101]$  direction. The upper part of the lattice (top-left pattern) shifts a distance of  $\tau d_A$  (where  $d_A$  is the edge length) and forms the configuration given in the top right. A larger view of the former pattern is given at the bottom. (b) Tenfold irrational twinning showing an aperiodic pattern in the central area. The dark-lined pattern is obtained from the connection of pentagon rings.

twin plane but periodical along the perpendicular direction (figure 7(b)). A row of large pentagons is obtained.

If one part of the initial  $O_1$  lattice (top-left pattern of figure 8(a)) is slipped along the  $[101]$  direction, the lattice will be transformed to the pattern schematized in the top right-hand side of figure 8(a). The bottom pattern of figure 8(a) shows the same configuration extended to a large area. The  $O_1$  lattice now has two orientations, the  $c$ -axis of which are separated by an angle of  $72^\circ$ . The parallel periodic sequence of irrational twinning cannot be carried out due to the different orientation of the twin plane (see broken lines laid out in the bottom pattern of figure 8(a)). This operation can lead to tenfold symmetry. Figure 8(b) shows the resulting pattern. In the central area and near the twin plane, the lattice is aperiodic and perfectly ordered, whereas the area between the twin planes is still that of the  $O_1$  phase.

## 5. Conclusion

The two-dimensional approximant patterns perpendicular to the pseudo tenfold axis were obtained from the HREM images as a result of the presence of recognizable pentagon units. The space groups of two orthorhombic phases found in  $Al_{80.75}Mn_{13.75}Ni_{5.5}$  and  $Al_{67}Cu_9Fe_{10.5}Cr_{10.5}Si_3$  were sorted out accordingly as  $Bbm2_1$  ( $a = 24 \text{ \AA}$ ,  $b = 12.4 \text{ \AA}$  and  $c = 32.7 \text{ \AA}$ ) and  $P2mc$  ( $a = 23.6 \text{ \AA}$ ,  $b = 12.3 \text{ \AA}$  and  $c = 20 \text{ \AA}$ ) respectively. Three kinds of crystallographic rearrangement mechanisms were proposed to explain the two-dimensional lattice transformations between approximant arrays and approximant/aperiodic arrays. The first

transformation is a linear translational slip. This slip distorts the initial lattice without changing the area of the unit cells. The second transformation can be divided into three types: rotational slip, screw rotational slip (rotational slip plus a displacement in the pseudo tenfold direction) and reflected rotational slip. The first two concern the rotation of three pentagons located inside a pentagon ring formed by nine pentagons around the rotation axis (the pseudo tenfold axis of the approximants) with a rotation angle of  $n\pi/5$ ,  $n = \text{integer}$ . The third type is also a screw rotational slip with a rotation angle of  $180^\circ$ . This rotation is restricted to a tiling fragment in which a convex pentagon is placed between a concave pentagon and a prolate rhombus. These operations can be carried out along any axis of the periodic approximant lattice to generate an infinite number of approximant phases. However, the aperiodic tiling in either one dimension or two dimensions cannot be generated by a simple slip applied on a periodic lattice. The formation of these quasicrystals involves the third mechanism, irrational twinning with a twin plane on an irrational atomic plane. A periodic sequence of irrational twinning in a periodic lattice generates the one-dimensional aperiodic lattice. In contrast, a tenfold irrational twinning generates the two-dimensional quasiperiodic lattice.

### Acknowledgment

We are most grateful to Dr C Dong for discussion and a critical reading of the manuscript.

### References

- [1] Bendersky L 1985 *Phys. Rev. Lett.* **55** 1461
- [2] Penrose R 1974 *Bull. Inst. Math. Appl.* **10** 266
- [3] van Tendeloo G, Van Landuyt J, Amelinckx S and Ranganathan S 1988 *J. Microsc.* **149** 1
- [4] Dong C and Dubois J M 1991 *J. Mater. Sci.* **26** 1647
- [5] He L X, Wu Y K, Meng X M and Kuo K H 1990 *Phil. Mag. Lett.* **61** 15
- [6] Audier M, Launois P, Denoyer F, Lambert M, Dong C and Dubois J M 1990 *Microsc. Microanal. Microstruct.* **1** 417
- [7] Dong C, Dubois J M, Kang S S and Audier M 1992 *Phil. Mag.* **65** 107
- [8] Beeli C, Nissen H-U and Robadey J 1991 *Phil. Mag. Lett.* **63** 87
- [9] Duneau M and Katz A 1985 *Phys. Rev. Lett.* **54** 2688
- Kalugin P A, Kitaev A and Levitov L 1985 *J. Physique* **46** 1601
- Elser V and Henley C L 1985 *Phys. Rev. Lett.* **55** 2883
- [10] Edagawa K, Suzuki K, Ichihara M and Takeuchi S 1991 *Phil. Mag.* **B 64** 629
- [11] Launois P, Audier M, Dénoyer F, Dong C, Dubois J M and Lambert M 1991 *Europhys. Lett.* **13** 629
- [12] Steurer W and Kuo K H 1990 *Phil. Mag. Lett.* **62** 175
- [13] Kang S S and Dubois J M 1992 *J. Phys.: Condens. Matter* submitted
- [14] Black P J 1955 *Acta Crystallogr.* **8** 43
- [15] Robinson K 1954 *Acta Crystallogr.* **7** 494
- [16] Hyde B G, Andersson S, Bakker M, Plug C M and O'Keeffe M 1979 *Prog. Solid State Chem.* **12** 273
- [17] Andersson S and Hyde B G 1974 *J. Solid-State Chem.* **9** 92
- [18] Dubois J M 1985 *J. Physique Coll.* **46** C8 335
- [19] Zhang H and Kuo K H 1990 *Phys. Rev. B* **42** 8907
- [20] Dong C and Dubois J M 1992 *J. Non-Cryst. Solids* submitted
- [21] Kang S S, Malaman B, Venturini G and Dubois J M 1991 *Acta Crystallogr.* at press
- [22] Mackay L 1982 *Physica A* **114** 609
- Levine D and Steindhart P J 1984 *Phys. Rev. Lett.* **53** 2477



Kramer P and Neri R 1984 *Acta Crystallogr. A* **40** 580

[23] Daulton T L, Kelton K F and Gibbons P C 1991 *Phil. Mag.* B **63** 687

[24] Hyde B G, Bagshaw A N, Andersson S and O'Keeffe M 1974 *Ann. Rev. Mater. Sci.* **4** 1